

Preclinical Evaluation of ^{18}F -JNJ64349311, a Novel PET Tracer for Tau Imaging

Lieven Declercq¹, Frederik Rombouts², Michel Koole³, Katleen Fierens⁴, Jonas Mariën², Xavier Langlois², José Ignacio Andrés⁵, Mark Schmidt⁶, Gregor Macdonald², Diederik Moechars², Wim Vanduffel⁷, Thomas Tousseyn⁸, Rik Vandenberghe⁹, Koen Van Laere³, Alfons Verbruggen¹ and Guy Bormans¹

¹Laboratory for Radiopharmacy, Department of Pharmaceutical and Pharmacological Sciences, KU Leuven, Leuven, Belgium; ²Neuroscience Discovery, Janssen Research and Development, a division of Janssen Pharmaceutica NV, Beerse, Belgium; ³Nuclear Medicine & Molecular Imaging, Department of Imaging and Pathology, KU Leuven and University Hospital Leuven, Leuven, Belgium; ⁴Discovery Sciences, Janssen Research and Development, a division of Janssen Pharmaceutica NV, Beerse, Belgium; ⁵Discovery Sciences, Janssen Research and Development, a division of Janssen-Cilag NV, Toledo, Spain; ⁶Janssen Early Development, a division of Janssen Pharmaceutica NV, Beerse, Belgium; ⁷Laboratory for Neuro- and Psychophysiology, Department of Neurosciences, KU Leuven, Leuven, Belgium; ⁸Translational Cell & Tissue Research, Department of Imaging & Pathology, KU Leuven, Leuven, Belgium and ⁹Laboratory for Cognitive Neurology, Department of Neurosciences, KU Leuven, Leuven, Belgium

Word Count: 6196

Corresponding author: Diederik Moechars, Neuroscience Discovery, Janssen Research and Development, a division of Janssen Pharmaceutica NV, Turnhoutseweg 30, 2340 Beerse, Belgium. E-mail: dmoear@its.jnj.com

First author: Lieven Declercq (research fellow), Laboratory for Radiopharmacy,
Faculty of Pharmaceutical Sciences, KU Leuven, Herestraat 49 - box 821, 3000
Leuven, Belgium. E-mail: lieven.declercq@kuleuven.be

Running title: ^{18}F -JNJ311: a Novel Tau PET Ligand

Abstract

In this study we have synthesized and evaluated ^{18}F -JNJ64349311, a tracer with high affinity for aggregated tau (K_i value of 8 nM) and high ($\geq 500x$) *in vitro* selectivity for tau over β -amyloid, in comparison with the benchmark compound ^{18}F -AV1451 (^{18}F -T807) in mice, rats and a rhesus monkey. **Methods:** Using autoradiography studies *in vitro* binding characteristics were determined on Alzheimer's disease (AD), Progressive supranuclear palsy (PSP) and Corticobasal degeneration (CBD) patient brain tissue slices. *Ex vivo* biodistribution studies were performed in mice. Radiometabolites were quantified in brain and plasma of mice and in plasma of a rhesus monkey using high performance liquid chromatography. Dynamic micro positron-emission tomography (μPET) studies were performed in rats and in a rhesus monkey to evaluate tracer pharmacokinetics in brain. **Results:** Mouse biodistribution studies showed moderate initial brain uptake and rapid brain wash-out. Radiometabolite analyses after injection of ^{18}F -JNJ64349311 in mice showed the presence of a polar radiometabolite in plasma, but not in brain. Semi-quantitative autoradiography studies on post-mortem tissue sections of human AD brains showed highly displaceable binding to tau-rich regions. No specific binding was, however, found on human PSP and CBD brain slices. μPET -scans on Wistar rats revealed moderate initial brain uptake (standardized uptake value, SUV of ~ 1.5 at 1 min p.i.) and rapid brain wash-out. Gradual bone uptake was, however, also observed. Blocking and displacement did not affect brain time-activity curves, suggesting no off-target specific binding of the tracer in healthy rat brain. A μPET scan on a rhesus monkey revealed moderate initial brain uptake (SUV of 1.9 at 1 min p.i.) with a rapid wash-out. In monkey, no bone uptake was detected during the 120-min scan. **Conclusion:** This biological evaluation suggests that ^{18}F -JNJ64349311 is a promising tau PET tracer candidate, with a favourable pharmacokinetic profile as compared to ^{18}F -AV1451.

Key Words: Alzheimer's disease, Progressive supranuclear palsy, Corticobasal degeneration, tau, PET, biomarker, PHFs, brain, diagnostic, ^{18}F -JNJ64349311, ^{18}F -AV1451.

INTRODUCTION

Despite huge efforts over the last few decades, more than 99% of drug candidates tested against AD, aiming at slowing disease progression and/or symptomatic improvement, ultimately failed in late stage development clinical trials (1). The pharmacological mechanism may simply not have been translated to therapeutic benefit in many cases; however another major problem has been reliance on clinical diagnosis for subject selection. The availability of fluid and imaging biomarkers such as cerebrospinal fluid β -amyloid and PET using radioligands for β -amyloid plaques promises to greatly improve diagnosis, although there continues to be need for biomarkers predictive of decline. Tau (*tubulin associated unit*) protein markers gained increasing interest in the last years due to a close correlation of cerebral tau deposition with clinical symptoms in AD and other tauopathies (2). Indeed, the extent and distribution of tau deposition may be more specific to Alzheimer's dementia and predictive of decline in subjects at risk for dementia, compared to β -amyloid plaque density in the brain (3). The design of tau PET ligands, however, has proven to be challenging, because of the complexity of tau as a PET target. Under pathological conditions, tau is hyperphosphorylated, self-aggregates into paired helical filaments (PHF) and eventually forms tangles that also contain other proteins. Since tau exists in six different isoforms, is subject to various posttranslational modifications, and tangles can have many ultrastructural conformations, the development of a specific tau PET tracer able to target tau pathology in AD remains daunting (4). Nonetheless, several tau-specific PET ligands have been developed in the past decade and they were recently discussed in a review by Dani et al. (5). Among the first of these identified was T807, a tracer developed by Siemens and then licensed to Eli Lilly, now known as ^{18}F -AV1451. This tracer is the most widely studied and the signal in brain has been demonstrated to follow Braak stages in cross-sectional studies of subjects at risk for

AD to full blown AD (6). However, it has some off-target binding (7) and exhibits a problematic kinetic profile, clearing slowly and failing to reach steady state in some brain regions (8-11). On the other hand, some reports demonstrated that ^{18}F -AV151 may also have some affinity for non-AD tauopathies (12). The aim of the present study was to develop a tau PET ligand with a superior pharmacokinetic profile as compared to ^{18}F -AV1451, but similar or better affinity and selectivity over β -amyloid plaques. We report here the *in vitro* and *in vivo* evaluation of ^{18}F -JNJ64349311 (^{18}F -JNJ311) by autoradiography studies on post-mortem human AD, PSP and CBD brain slices, biodistribution and radiometabolite studies in mice and μPET studies in rats and a rhesus monkey, in comparison with ^{18}F -AV1451.

MATERIALS AND METHODS

Synthesis and evaluation of the authentic reference compound of JNJ311 (including precursor) was published in detail elsewhere (13), as well as the medicinal chemistry resulting in the discovery of this fluorinated compound. The precursor for radiosynthesis of ^{18}F -AV1451 and the authentic reference material, and the nonradioactive reference material for AV680 and AV45 were synthesized by Janssen Research & Development (Janssen Pharmaceutica NV, Beerse, Belgium) following literature reports (14). All other chemicals and reagents were purchased from commercial sources and used without further purification. The distribution-coefficient ($\text{LogD}_{7.4}$) of JNJ311 was determined by Sirius Analytical Instruments (Forest Row, U.K.) according to a previously described report (15). Calculated polar surface area (PSA) was obtained using MarvinSketch (ChemAxon, version 6.1.0). For analysis of radiolabeled compounds, the high performance liquid chromatography (HPLC) column eluate, after passing through the ultraviolet detector, was led over a 3-inch NaI(Tl) scintillation detector connected to a single channel analyser (GABI box; Raytest,

Straubenhardt, Germany). Data were acquired and analysed using a GINA Star data acquisition system (Raytest). Quantification of radioactivity in samples of biodistribution and radiometabolite studies was performed according to a previously reported procedure (14). Quantitative data are expressed as mean \pm standard deviation. Means were compared using an unpaired two-tailed student t-test. Values were considered statistically significant for $P \leq 0.05$. Post-mortem human AD brain slices were provided by University Hospitals Leuven (10- μ m thick; Neurology Department, Leuven, Belgium), after approval from the local Institutional Review Board. Post-mortem human CBD and PSP brain slices were provided by Janssen Research and Development (10- μ m thick; Neuroscience Biology Department, Belgium), after approval from the Use Committee of Janssen Pharmaceutical Companies of Johnson & Johnson and the local ethical committee. Animals were housed in individually ventilated cages in a thermo-regulated (~ 22 °C), humidity-controlled facility under a 12 h - 12 h light-dark cycle, with access to food and water ad libitum. All animal experiments were conducted according to the Belgian code of practice for the care and the use of animals, after approval from the university animal ethics committee.

Radiosynthesis

^{18}F -fluoride ($^{18}\text{F}^-$) was produced and purified according to a previously described procedure (14). A solution of 0.5 mg of trimethylammonium precursor (mono- or tris-trifluoroacetate salts) in 0.3 mL DMF was added to the dried $^{18}\text{F}/\text{K}_2\text{CO}_3/\text{K}-222$ residue and the mixture was heated at 120 °C for 10 min. The crude radiolabeling mixture was diluted with 0.6 mL mobile phase and purified using reverse phase HPLC (RP-HPLC) on an XBridge C_{18} column (5 μ m, 4.6 mm x 150 mm; Waters) eluted with a mixture of 0.01 M Na_2HPO_4 pH 9.6 and EtOH (65:35 v/v) at a flow rate of 0.8 mL/min and with ultraviolet detection at 254 nm. The purified radiotracer solution was diluted with

saline to obtain an ethanol concentration <10%, suitable for intravenous (i.v.) injection. The solution was subsequently passed through a 0.22- μm filter (Millex-GV, Millipore, Billerica, MA, U.S.A.) to obtain a sterile product. Quality control was performed using RP-HPLC on an XBridge column (C_{18} , 3.5 μm , 3.0 mm x 100 mm; Waters) eluted with a mixture of 0.01 M Na_2HPO_4 pH 9.6 and CH_3CN (70:30 v/v) at a flow rate of 0.8 mL/min. Ultraviolet detection was performed at 254 nm. ^{18}F -AV1451 was radiolabeled according to a previously reported procedure (14).

Biodistribution studies

Biodistribution studies were carried out in healthy male Naval Medical Research Institute (NMRI) mice (body weight: 30-40 g) at 2, 10, 30 and 60 min post injection (p.i.) ($n = 3/\text{time point}$) according to a previously reported procedure (14). SUVs were calculated as (counts per minute in body part/weight of the body part in g) / (sum of counts per minute in all body parts/body weight in g).

Autoradiography studies

Air-dried frozen, 10- μm thick post-mortem slices of an AD patient (visual cortex of a 68-y-old female with Braak stage VI), PSP patient (frontal cortex of a 71-y-old female) and CBD patient (frontal cortex of a 74-y-old female) were incubated for 60 min in a solution of tracer (740 kBq/500 μL per section) and subsequently washed with mixtures of phosphate buffered saline and ethanol as described elsewhere (16). To assess specificity of binding, slices were incubated with radiotracer in the presence of 1 μM of authentic reference compound, AV680 or AV45 (the latter two compounds were only used on the AD brain slices). After drying, slices were exposed to a phosphor storage screen (super-resolution screen, Perkin Elmer, Waltham, MA, U.S.A.). Screens were read in a Cyclone Plus system (Perkin Elmer) and analyzed

using Optiquant software. Results are expressed as digital light units per square mm (digital light units/mm²).

Phosphorylated PHF tau and β -amyloid plaques isolation from human AD brain

Enriched PHF tau and β -amyloid plaques fractions were prepared as previously described (14), using post-mortem human AD brain tissue with high tau fibril and/or high β -amyloid plaque load, respectively.

In vitro competitive radioligand binding assays

The competitive radioligand binding assays measure the binding of a fixed amount of ³H-AV680 (PHF tau binder) or ³H-AV45 (β -amyloid plaques binder) in the presence of a concentration range of test compounds following a described experimental assay setup (14).

Immunohistochemistry

Adjacent AD, PSP or CBD slices were used for immunohistochemistry to correlate with radiotracer binding. Sections were first dried, fixed in 4% formaldehyde, treated for 5 min with hydrogen peroxide (5%, DAKO S2023, Glostrup, Denmark) and permeabilized with phosphate buffer containing 0.3% Triton X-100, followed by a 1-h incubation immunostaining with anti-tau (AT8, in-house made; 0.4 μ g/mL) or anti- β -amyloid antibodies (4G8, 2 μ g/mL, Eurogentec SIG-39200, Fremont, CA, U.S.A.) in the AD case. After extensive washing, slices were incubated during 30 minutes with horseradish peroxidase conjugated anti-mouse secondary antibody (DAKO, K4000, Envision, Glostrup, Denmark), followed by chromogenic 3,3-diaminobenzidine (DAB) labeling (DAKO, K3468). Finally, sections were counterstained with hematoxylin,

dehydrated and mounted with permanent mounting medium (Vectamount H-5000, Vector Laboratories, Burlingame, CA, U.S.A.).

Radiometabolite studies

Perfused brain radiometabolites. Study was carried out in NMRI mice at 10 or 60 min p.i. ($n = 3$ /time point) according to a previously described procedure (14). HPLC analysis was performed on a C₁₈ column (XBridge 3.5 μ m, 3.0 mm x 100 mm; Waters) eluted with a mixture of 0.01 M Na₂HPO₄ pH 9.6 and CH₃CN (77:23 v/v) at a flow rate of 0.7 mL/min.

Plasma radiometabolites in mice. NMRI mice were anesthetized with isoflurane (2.5% in O₂ at 1 L/min flow rate) and injected with ¹⁸F-JNJ311 (~3.7 MBq) via a lateral tail vein. Mice were sacrificed by decapitation at 2, 10, 30 or 60 min p.i. ($n = 3$ /time point). Blood was collected in EDTA containing tubes (4-mL tubes; BD vacutainer, BD, Franklin Lakes, NJ, U.S.A.), weighed, counted for radioactivity in the γ -counter and stored on ice. Blood was subsequently centrifuged at 2330 x g for 10 min to separate the plasma. Plasma (0.5 mL) was weighed, counted for radioactivity in a γ -counter and spiked with 20 μ g of authentic JNJ311. Afterwards, proteins in the plasma sample were precipitated by adding an equal volume of CH₃CN followed by centrifugation for 5 min at 2330 x g. Next, supernatant (0.5 mL) was collected, diluted with H₂O (0.7 mL) and filtered through a 0.22- μ m filter (Nylon Acrodisc, 13 mm Syringe filter, Pall Life Sciences). The sample was counted for radioactivity in the γ -counter, before being analyzed by HPLC (Waters XBridge C₁₈ column, 3.5 μ m, 3.0 mm x 100 mm; eluted with a mixture of 0.01 M Na₂HPO₄ pH 9.6 and CH₃CN (77:23 v/v) at a flow rate of 0.7 mL/min). Ultraviolet detection was done at 254 nm. The

HPLC eluate was collected as 1-mL fractions and their radioactivity was counted in an automated γ -counter.

μ PET imaging studies

Wistar rats. Dynamic 120-min μ PET scans with all tracers were acquired on a Focus 220 μ PET scanner (Concorde Microsystems, Knoxville, TN, U.S.A.) on three female Wistar rats simultaneously, which were scanned three times. The rats were kept under gas anaesthesia during the whole procedure (2.5% isoflurane in O₂ at 1 L/min flow rate). Scans were acquired in list mode and acquisition data were Fourier rebinned in 27 time frames (4 x 15 s, 4 x 60 s, 5 x 180 s, 8 x 300 s, 6 x 600 s). Data, which were 3D maximum a posteriori (3D-MAP) reconstructed, were manually aligned with a rat brain ¹⁸F-FDG template in Paxinos coordinates using an affine transformation, to allow predefined volumes of interest analysis (17). Time-activity curves (TACs) of the whole brain were generated using volumes of interest analysis with PMOD software (v 3.2, PMOD Technologies, Zürich, Switzerland). Radioactivity concentration in the brain was expressed as SUV (calculated as (radioactivity in Bq in brain/mL) / (total injected dose (Bq)/body weight in g)) as a function of time after tracer injection. Scans were started immediately after i.v. injection of about 50 MBq of radiotracer. For pre-treatment and displacement studies, solutions of cold reference compounds JNJ311 or AV1451 dissolved in a mixture of 5% DMSO, 5% Tween 80 and 40% (2-hydroxypropyl)- β -cyclodextrin, filtered through a 0.22- μ m membrane filter (Millex-GV, Millipore), were used. Pre-treatment ($n = 3$) was done by subcutaneous (s.c.) injection of 10 mg/kg of JNJ311 or AV1451, 60 min prior to radiotracer injection. Displacement ($n = 3$) was performed by i.v. injection of 1 mg/kg JNJ311 or AV1451 30 min after radiotracer injection. μ PET-images were compared to a baseline scan ($n = 3$), acquired in a non-treated rat. A vehicle control study with ¹⁸F-AV1451 was

performed to assess the possible influence of the vehicle during the pre-treatment and displacement study.

Rhesus monkey. A dynamic 120-min μ PET scan with ^{18}F -JNJ311 or ^{18}F -AV1451 was performed with a Focus 220 μ PET scanner on a male rhesus monkey (6 y-old *Macaca mulatta*, 7.6 kg), that was sedated with ketamine (Ketalar[®]) and xylazine (Rompun[®]) *via* intramuscular injection. During scanning the monkey received repeatedly an additional dose of ketamine/xylazine *via* i.v. injection. O₂ saturation in blood, breathing frequency and heartbeat frequency were monitored during the entire experiment. The head of the animal was placed central in the field of view of the μ PET scanner. Scans were acquired in list mode and Fourier rebinned in 27 time frames (4 x 15 s, 4 x 60 s, 5 x 180 s, 8 x 300 s, 6 x 600 s). Data were reconstructed using a 3D-MAP iterative reconstruction. TACs of the whole brain were generated using volumes of interest analysis with PMOD software. Radioactivity concentration in the brain is expressed as SUV as a function of time after tracer injection. Scans were started immediately after i.v. injection of 185 MBq of ^{18}F -JNJ311 or ^{18}F -AV1451 *via* the vena saphena of the right leg. Blood samples were collected at 10, 30 and 60 min p.i. *via* a catheter in the vena saphena of the left leg and plasma was analysed for radiometabolites according to the same procedure as for mice (see above).

RESULTS

Human PK predictions for JNJ311

A human PK prediction was made based on a PK study in mouse, rat and dog (0.25 mg/kg, i.v.). The results are summarized in Supplemental Table 1. Using the Dedrick approach a biphasic clearance in human was predicted in which a fast clearance of 1.05 mL/min/kg was predicted for the initial phase, resulting in a short half-life of 0.7 h

(18). With allometric scaling, a high but slightly slower monophasic clearance of 1.285 mL/min/kg was predicted for humans, corresponding to a half-life of 2.4 h. Both models hence predicted JNJ311 to have a sufficiently fast clearance in humans following i.v. dosing, based on pharmacokinetic data in mouse, rat and dog following i.v. administration.

Radiolabeling

^{18}F -JNJ311 (Fig. 1) was synthesized by a nucleophilic substitution reaction with ^{18}F -fluoride on its trimethylammonium precursor. Heating of the precursor solution with ^{18}F -fluoride in the presence of K-222/ K_2CO_3 afforded ^{18}F -JNJ311 ($n = 6$) with an average, decay-corrected, radiochemical yield of 46% (relative to total radioactivity of fluorine-18 in the preparative chromatogram). Radiochemical yields were identical for the mono- and tris-trifluoroacetate (TFA) salt of the precursor of ^{18}F -JNJ311. The radiochemical purity was more than 98%. ^{18}F -JNJ311 was obtained within a total synthesis time of 60 min. The specific activity ^{18}F -JNJ311 was 81 ± 72 GBq/ μmol at the end of synthesis. ^{18}F -AV1451 was collected within a total synthesis time of 60 min with a specific activity of 45 ± 35 GBq/ μmol at the end of synthesis ($n = 4$) and a radiochemical purity greater than 95%.

Mouse biodistribution studies

Supplemental Table 2 shows SUVs of ^{18}F -JNJ311 and ^{18}F -AV1451 in different organs at 2, 10, 30 and 60 min p.i. High SUVs were recorded for the liver and kidneys, due to the hepatobiliary and renal plasma clearance of both compounds. Radioactivity concentration in blood decreased rapidly over time for ^{18}F -JNJ311 and ^{18}F -AV1451 (SUVs of, respectively, 0.5 and 0.4 at 2 min p.i. and this cleared to 0.1 and 0.2 by 60 min p.i.). Rapid and moderate initial brain uptake was recorded, with a SUV of,

respectively, 1.9 and 2.2 for ^{18}F -JNJ311 and ^{18}F -AV1451 at 2 min p.i. Brain wash-out was comparable for ^{18}F -JNJ311 and ^{18}F -AV1451 with SUVs around 0.1 at 60 min p.i. ^{18}F -JNJ311 showed the highest 2-to-60 min brain radioactivity ratio (2-to-60 min brain ratio of 29.6), whereas ^{18}F -AV1451 had a lower 2-to-60 min brain ratio (18.3, $p < 0.05$). Bone uptake was minimal and remained stable over time for both tracers.

In vitro autoradiography binding studies

Digital autoradiography with ^{18}F -JNJ311 on post-mortem human AD brain slices showed binding to tau pathology-rich regions in the visual cortex (Fig. 2). No specific binding to tau pathology was, however, seen in the frontal cortex on the post-mortem human PSP and CBD brain slices (Supplemental Fig. 1). Immunohistochemistry with tau and β -amyloid antibodies, performed on adjacent slices, identified numerous PHF and neuritic plaque deposits, confirming co-localization of tracer binding with PHFs in AD (Supplemental Fig. 2), but not in the PSP or CBD brain slices (Supplemental Fig. 3). To assess the specificity of the tracer binding to PHFs, blocking studies with authentic JNJ311, AV45 or AV680 were performed. Self-block studies with 1 μM of cold JNJ311 resulted in 90% inhibition ($n = 3$) in the AD brain slices, but only 14% and 10% inhibition ($n = 3$) in, respectively, the PSP and CBD brain slices. Binding of ^{18}F -JNJ311 was reduced with 96% in the presence of 1 μM AV680 compared to control ($n = 3$) in the AD brain slices. Blocking of ^{18}F -JNJ311, on the other hand, with 1 μM of AV45 led to a blocking percentage of only 7% ($n = 3$) in the AD brain slices. Blocking percentages were calculated as (digital light units/ mm^2 in the presence of 1 $\mu\text{mol/L}$ blocker) / (digital light units/ mm^2 tracer only).

In vitro competitive radioligand binding assays

Binding assays with ^3H -AV680 in the presence of the cold test compounds showed high affinity of JNJ311 for enriched aggregated tau from human AD brain samples with a K_i value of 8 nM (Supplemental Table 3). In the competition assays with ^3H -AV45, only AV1451 and AV45 showed specific binding with a K_i value of 278 nM and 12 nM, respectively. JNJ311 and AV680 on the other hand, had K_i values higher than 4398 nM.

Radiometabolites

Plasma radiometabolite analysis after i.v. administration of ^{18}F -JNJ311 in NMRI mice and a rhesus monkey revealed fast radiotracer metabolism. Thirty minutes after injection 22% and 35% of the recovered radioactivity corresponded to intact tracer in mice and the rhesus monkey, respectively (Supplemental Table 4). All detected radiometabolites were more polar than the intact tracer at 60 min p.i. The recovery of the HPLC column-injected radioactivity for ^{18}F -JNJ311 was 95% for mice ($n = 12$) and 90% for the rhesus monkey ($n = 3$). In brain, the percentage of intact ^{18}F -JNJ311 remained close to 100% at both 10 and 60 min p.i. (Supplemental Table 4). The recovery of the HPLC column-injected radioactivity for ^{18}F -JNJ311 in brain extract was 90% ($n = 6$).

μPET imaging studies

Wistar rats. Results of the 120-min baseline, pre-treatment and displacement study are shown in Figure 3. Time-activity curves (TACs) of the baseline scans of both ^{18}F -JNJ311 and ^{18}F -AV1451 show moderate initial brain uptake, with a comparably moderate SUV in brain of ~ 1.5 at 1 min p.i. ^{18}F -JNJ311 had the fastest brain wash-out rate (SUV of 0.2 ± 0.04 at 60 min p.i.) as shown in the $\% \text{SUV}_{\text{max}}$ curves (Supplemental Fig. 4). Bone uptake was observed for both compounds at later time points, most likely

due to defluorination (Fig. 3). No self-blocking or self-displacement effect was observed for ^{18}F -JNJ311 ($p > 0.05$ at all time points), indicating absence of specific not tau related binding in brain. Lower brain uptake of ^{18}F -AV1451 during the baseline scan, compared to the pre-treatment study was observed ($p < 0.05$ at 5 min p.i.). An increase of brain activity was also observed after injection of a displacement dose at 30 min p.i. for ^{18}F -AV1451 ($p < 0.05$ at 38 min p.i.). No such differences were, however, recorded during a vehicle control study with ^{18}F -AV1451 (Supplemental Fig. 5).

Rhesus monkey. Results of the 120-min baseline scan of ^{18}F -JNJ311 and ^{18}F -AV1451 are shown in Figure 4. TACs of the baseline scan of ^{18}F -JNJ311 in the brain show a fast, moderate initial brain uptake with a rapid wash-out (SUV of 1.9, time to peak: 1 min) and low white matter binding was recorded. TACs of the baseline scan of ^{18}F -AV1451 in the brain show a slower initial brain uptake (SUV of ~ 1.3 , time to peak uptake: 15 min) and wash-out (Supplemental Fig. 6). TACs of the skull show that the SUV signal did not increase as a function of time for both compounds.

DISCUSSION

The aim of this study was the development of a selective aggregated fluorine-18 labeled tau PET ligand, with fast clearance from the brain. The medicinal chemistry optimization that resulted in the selection of JNJ311 as the best tau PET candidate (based on *in vitro* and *in vivo* data) was published elsewhere (13). In the present study we describe the preclinical evaluation of this tau PET ligand, in comparison with ^{18}F -AV1451. JNJ311 was selected based on its high affinity for aggregated tau (K_i value of 8 nM) and high specificity for tau over β -amyloid (more than 500x selective). JNJ311 was radiolabeled with fluorine-18 and the resulting radiotracer was evaluated in mice, rats and in a rhesus monkey. Semi-quantitative autoradiography experiments were used

to evaluate binding characteristics in human AD, PSP and CBD pathology. Such autoradiography studies are needed in order to determine the affinity for tau pathology in its 'natural AD, PSP or CBD environment'. 3R tauopathies, such as Pick's disease, were not tested in this stage of tracer development, due to the low prevalence of tau inclusions in frontotemporal dementia (19). Results revealed high and selective binding to tau pathology in post-mortem slices of the visual cortex for ^{18}F -JNJ311 in an AD patient in the latest Braak stage. No specific binding, on the other hand, could be demonstrated in the case of PSP or CBD pathology. To assess the specificity of the tracer binding to the tau pathology, self-blocking studies with the authentic reference compound JNJ311 and, in the AD case, also blocking studies with the structurally unrelated tau ligand AV680 and the specific β -amyloid ligand AV45 were performed. AV680 was used as the benchmark compound in this experiment, due to its higher selectivity for aggregated tau over β -amyloid and lower off-target binding than AV1451 (20). AV45 was used in the blocking studies to assess the specificity of JNJ311 for tau over β -amyloid. Self-block resulted in 90% inhibition in the cortical layers, which demonstrates that the binding of ^{18}F -JNJ311 was specific. No specific binding could, however, be demonstrated in the frontal cortex of, respectively, PSP and CBD. Binding of ^{18}F -JNJ311 was also reduced with more than 79% in the presence of 1 μM AV680 on the AD brain slices, indicating tau-specific binding. Finally, blocking with AV45 resulted in only 7% displacement of ^{18}F -JNJ311, confirming that JNJ311 binds more selectively to tau pathology in the AD brain slices. Furthermore, immunohistochemistry performed on adjacent slices identified numerous hyperphosphorylated tau and neuritic plaque deposits in the cortical layers, with a pattern that, in the case of AD, visually correlated with the autoradiographic images, confirming co-localization of tracer binding with hyperphosphorylated tau in AD, but not in PSP and CBD. The lack of binding of ^{18}F -JNJ311 in the latter two tauopathies

can most likely be explained by the ultrastructural differences, but also the different tau fractions that exist between these tauopathies and AD (12), which may significantly change JNJ311s binding site. Only one brain sample was, however, tested in the case of PSP and CBD. Another limitation of the PSP autoradiography study is the lower prevalence of tau inclusions in the frontal cortex, compared to the subthalamic nucleus, basal ganglia or brainstem (12). A favourable pharmacokinetic profile is an important factor in the development of a PET tracer, but with a $\log D_{7,4}$ value of 2.2 and a PSA value of 51 \AA^2 , ^{18}F -JNJ311 has appropriate properties to efficiently pass the blood-brain barrier (21). This assumption was confirmed in the biodistribution studies in mice, since ^{18}F -JNJ311 displayed a moderate initial blood-brain barrier passage (SUVs of 1.9 at 2 min p.i.). ^{18}F -JNJ311 also revealed a rapid brain wash-out (SUV of 0.1 at 60 min p.i.). ^{18}F -JNJ311 displayed hereby a similar brain uptake and wash-out as ^{18}F -AV1451 (SUVs of 2.2 at 2 min p.i. and 1.0 at 10 min p.i.); this was demonstrated by the 2-to-60 min brain activity ratio, which was 30 for ^{18}F -JNJ311, higher than for ^{18}F -AV1451 (value of 18; $p < 0.05$), indicating a faster brain wash-out for ^{18}F -JNJ311 in mice. No pronounced bone uptake at 60 min p.i. was also revealed in NMRI mice.

Further *in vivo* evaluation ^{18}F -JNJ311 was done by performing small-animal μPET studies in Wistar rats. TACs of the μPET scans with ^{18}F -AV1451 show a similar brain uptake as those with ^{18}F -JNJ311 in rats. No noticeable influence on the brain TACs was observed for self-blocking and self-displacement of ^{18}F -JNJ311 ($p > 0.05$ for all time points for) in rats, which indicates that there was no non-tau related specific binding in brain, in line with extensive CEREP and DiscoverX profiling (results in the preclinical *in vitro* characterisation study, which will be published elsewhere). On the other hand, lower brain uptake of ^{18}F -AV1451 was recorded during the baseline scan, compared to the pre-treatment study ($p < 0.05$ at 5 min p.i.). This effect may be explained by saturation of metabolic enzymes and/or plasma proteins leading to a

higher free fraction of ^{18}F -AV1451 available for brain uptake. A similar effect was seen in the displacement study with ^{18}F -AV1451 ($p < 0.05$ at 38 min p.i.). This possible interaction between the cold authentic reference compound AV1451 and ^{18}F -AV1451 may have consequences, since polypharmacy is common among AD patients (22), and this may potentially lead to decreased plasma clearance of ^{18}F -AV1451. The influence of drugs on the metabolism of ^{18}F -AV1451 could therefore possibly complicate its PET quantification and theoretically lead to false conclusions.

Fast clearance from brain, as seen in the latter biodistribution and μPET studies with ^{18}F -JNJ311, could be explained by the rapid metabolism (and thus rapid plasma clearance) observed for ^{18}F -JNJ311 in plasma of NMRI mice and the rhesus monkey (33% of intact tracer left 10 min p.i. for mice and 35% of intact tracer left 30 min p.i. for the monkey), with detection of one unidentified polar radiometabolite. This rapid plasma clearance was also seen in the human PK predictions for JNJ311 (Supplemental Table 1). The rate of metabolism was, however, considerably faster in mice than in the rhesus monkey (Supplemental Table 4). The detected radiometabolite was not able to pass the blood-brain barrier in mice, as the fraction of intact tracer remained high in brain homogenates over time (94% of intact tracer left at 60 min p.i.). Similar findings were published for ^{18}F -AV1451 (14), with detection of one polar metabolite in plasma that also did not pass the blood-brain barrier in mice, although the rate of metabolism was not as pronounced as for ^{18}F -JNJ311 (84% of intact ^{18}F -AV1451 left at 10 min p.i.).

The TACs of both ^{18}F -JNJ311 and ^{18}F -AV1451 of the monkey μPET study reveal a homogenous distribution of both compounds in all brain regions, with no increased uptake in the corpus callosum. TACs of the skull, of ^{18}F -JNJ311 and ^{18}F -AV1451, showed that the focally increased uptake around the skull cannot be attributed to bone uptake, related to ^{18}F -fluoride, as the signal declines over time (Fig. 4). These areas of

increased focal tracer uptake around the skull with the μ PET scan of ^{18}F -JNJ311 are probably related to fixation of an acrylic headpost to the skull of the monkey, used to position the head during MRI scanning. This headpost can cause inflammation and/or scar formation of the skin around the headpost. Excessive binding of ^{18}F -fluoride in the skull could complicate quantification of ^{18}F -JNJ311 in brain, due to partial volume effects, e.g. surrounding petrous bone spilling into the medial temporal cortex, but this bone uptake effect was thus only seen in rats and not in mice and the rhesus monkey. Since ^{18}F -AV1451 also showed significant bone uptake in rats, but not in mice and monkeys, both tracers seem susceptible to interspecies differences with regard to defluorination, as it is the case for many PET tracers (23,24).

The superior brain pharmacokinetic profile of ^{18}F -JNJ311 led to the selection of this tracer as the optimal candidate for further tau PET exploration. Although ^{18}F -JNJ311 also seems to show a superior pharmacokinetic profile in rats and monkey compared to ^{18}F -AV1451, clinical PET scans with ^{18}F -JNJ311 in AD patients are necessary to make a relevant comparison. Human pharmacokinetic predictions for JNJ311 were made based on a PK study in mouse, rat and dog (0.25 mg/kg, JNJ311) and indicate a fast clearance in man (Supplemental Table 1).

CONCLUSION

Based upon its *in vitro* and *in vivo* preclinical profiling, ^{18}F -JNJ64349311 is a promising candidate for quantitative tau PET imaging in AD with a favourable pharmacokinetic profile in comparison with the current benchmark ligands.

DISCLOSURE

This research was funded by Janssen Research & Development and the Institute for the Promotion of Innovation through Science and Technology in Flanders (IWT).

ACKNOWLEDGEMENTS

We thank Julie Cornelis, Jana Hemelaers (Laboratory for Radiopharmacy, KU Leuven) and Christophe Ulens (Laboratory for Neuro- and Psychophysiology, KU Leuven) for their skilful help with the animal experiments. We also gratefully acknowledge the help of Astrid Bottelbergs and Ilse Lenaerts (Neuroscience Discovery, Janssen Research and Development, a division of Janssen Pharmaceutica NV, Beerse) with the immunohistochemistry and ³H-autoradiography experiments. Finally, we would like to express our appreciation for the scientific advice of Hartmuth Kolb (head of Neuroscience Biomarkers at Janssen Research and Development, LaJolla, USA).

REFERENCES

1. Cummings JL, Morstorf T, Zhong K. Alzheimer's disease drug-development pipeline: few candidates, frequent failures. *Alzheimers Res Ther.* 2014;6:37.
2. Lee VM, Goedert M, Trojanowski JQ. Neurodegenerative tauopathies. *Annu Rev Neurosci.* 2001;24:1121-1159.
3. Braak H, Braak E. Neuropathological staging of Alzheimer-related changes. *Acta Neuropathol.* 1991;82:239-259.
4. Villemagne VL, Furumoto S, Fodero-Tavoletti M, et al. The challenges of tau imaging. *Future Neurol.* 2012;7:409-421.
5. Dani M, Brooks DJ, Edison P. Tau imaging in neurodegenerative diseases. *Eur J Nucl Med Mol Imaging.* 2015;43:1139-1150.
6. Schwarz AJ, Yu P, Miller BB, et al. Regional profiles of the candidate tau PET ligand 18F-AV-1451 recapitulate key features of Braak histopathological stages. *Brain.* 2016;139:1539-1550.
7. Lowe VJ, Curran G, Fang P, et al. An autoradiographic evaluation of AV-1451 Tau PET in dementia. *Acta Neuropathol Commun.* 2016;4:58.
8. Chien DT, Bahri S, Szardenings AK, et al. Early clinical PET imaging results with the novel PHF-tau radioligand [F-18]-T807. *J Alzheimers Dis.* 2012;34:457-468.
9. Baker SL, Lockhart SN, Price JC, et al. Reference tissue-based kinetic evaluation of 18F-AV-1451 in aging and dementia. *J Nucl Med.* 2016;116:1752-1753.
10. Shcherbinin S, Schwarz AJ, Joshi A, et al. Kinetics of the Tau PET Tracer 18F-AV-1451 (T807) in Subjects with Normal Cognitive Function, Mild Cognitive Impairment, and Alzheimer Disease. *J Nucl Med.* 2016;57:1535-1542.

11. Wooten D, Guehl NJ, Verwer EE, et al. Pharmacokinetic evaluation of the tau PET radiotracer [18F]T807 ([18F]AV-1451) in human subjects. *J Nucl Med.* 2016;Epub ahead of print.
12. Dani M, Brooks DJ, Edison P. Tau imaging in neurodegenerative diseases. *Eur J Nucl Med Mol Imaging.* 2016;43:1139-1150.
13. Rombouts FJ, Andres JI, Ariza M, et al. Discovery of N-(pyridin-4-yl)-1,5-naphthyridin-2-amines as potential tau pathology PET tracers for Alzheimer's Disease. *J Med Chem.* 2017;Epub ahead of print.
14. Declercq L, Celen S, Lecina J, et al. Comparison of new tau PET-tracer candidates with [18F]T808 and [18F]T807. *Mol Imaging.* 2016;15:1-15.
15. Gocan S, Cimpan G, Comer J. Lipophilicity measurements by liquid chromatography. *Adv Chromatogr.* 2006;44:79-176.
16. Xia CF, Arteaga J, Chen G, et al. [(18)F]T807, a novel tau positron emission tomography imaging agent for Alzheimer's disease. *Alzheimers Dement.* 2013;1-11.
17. Casteels C, Vermaelen P, Nuyts J, et al. Construction and evaluation of multitracer small-animal PET probabilistic atlases for voxel-based functional mapping of the rat brain. *J Nucl Med.* 2006;47:1858-1866.
18. Van den Bergh A, Sinha V, Gilissen R, et al. Prediction of human oral plasma concentration-time profiles using preclinical data: comparative evaluation of prediction approaches in early pharmaceutical discovery. *Clin Pharmacokinet.* 2011;50:505-517.
19. Graff-Radford NR, Woodruff BK. Frontotemporal dementia. *Semin Neurol.* 2007;27:48-57.
20. Shah M, Catafau AM. Molecular imaging insights into neurodegeneration: focus on tau PET radiotracers. *J Nucl Med.* 2014;55:871-874.

21. Pike VW. PET radiotracers: crossing the blood-brain barrier and surviving metabolism. *Trends Pharmacol Sci.* 2009;30:431-440.
22. Singh S, Kushwah AS, Singh R, Farswan M, Kaur R. Current therapeutic strategy in Alzheimer's disease. *Eur Rev Med Pharmacol Sci.* 2012;16:1651-1664.
23. Celen S, Koole M, De AM, et al. Preclinical evaluation of 18F-JNJ41510417 as a radioligand for PET imaging of phosphodiesterase-10A in the brain. *J Nucl Med.* 2010;51:1584-1591.
24. Sephton SM, Dennler P, Leutwiler DS, et al. Synthesis, radiolabelling and in vitro and in vivo evaluation of a novel fluorinated ABP688 derivative for the PET imaging of metabotropic glutamate receptor subtype 5. *Am J Nucl Med Mol Imaging.* 2012;2:14-28.

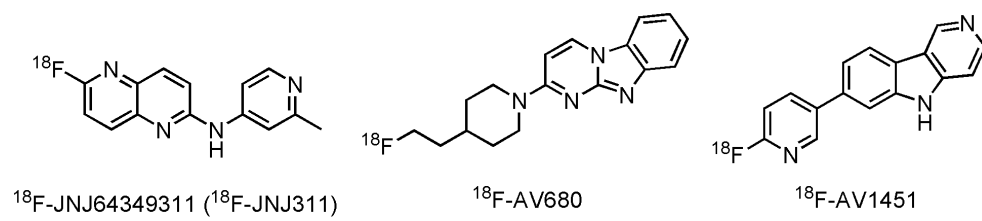


FIGURE 1. Chemical structures of ^{18}F -JNJ311, ^{18}F -AV1451 and ^{18}F -AV680.

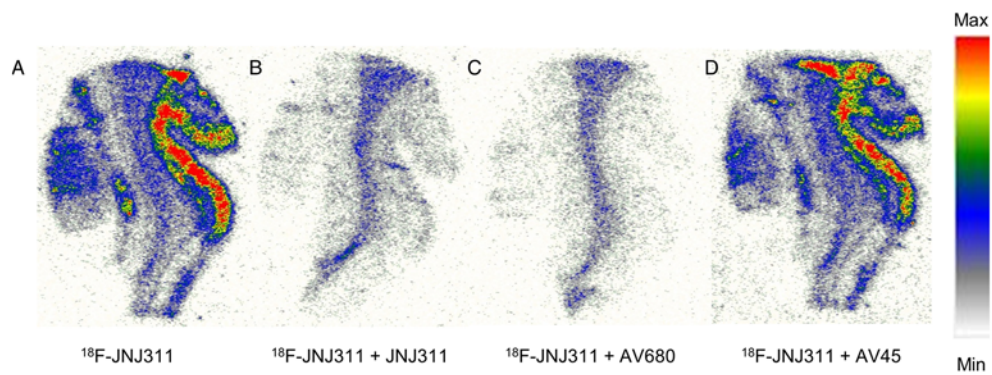


FIGURE 2. Adjacent, 10- μm -thick, post-mortem human AD brain slices of the visual cortex of an AD patient (68-year-old with Braak stage VI) incubated with ^{18}F -JNJ311 (740 kBq / 500 μL / slice) (A) in the presence of authentic reference compound JNJ311 (B), AV680 (C) or AV45 (D) at 1 $\mu\text{mol/L}$.

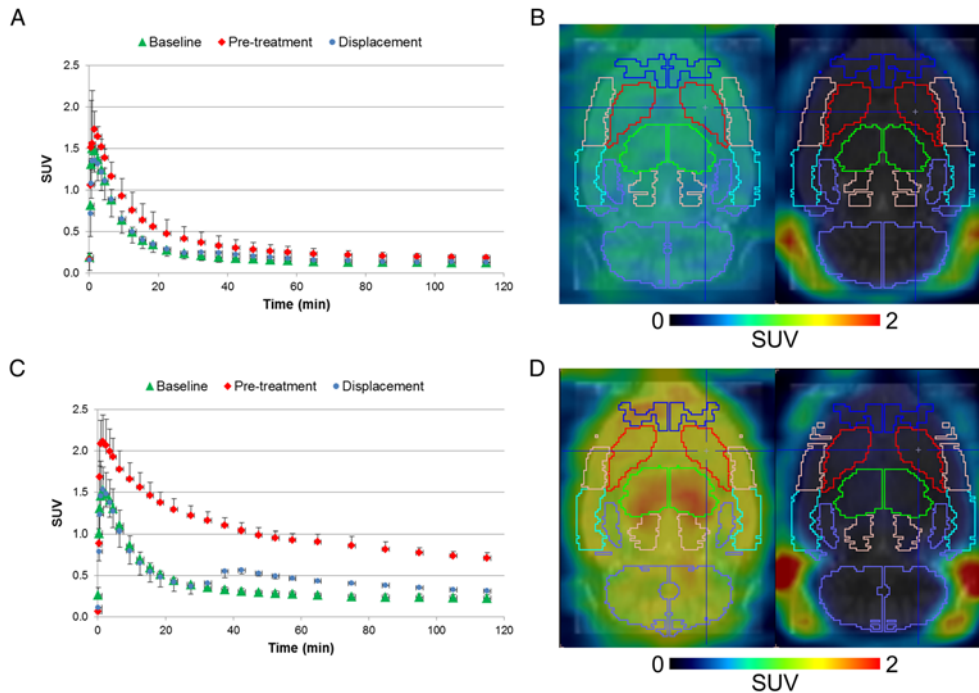


FIGURE 3. Whole brain μ PET time-activity curves for ^{18}F -JNJ311 (A) and ^{18}F -AV1451 (C) of three female Wistar rats. Baseline scan ($n = 3$ per tracer); pre-treatment experiment ($n = 3$ per tracer): cold JNJ311 (A and B) or AV1451 (C and D), 10 mg/kg injected subcutaneously 60 min prior to radiotracer injection and displacement study ($n = 3$ per tracer): cold JNJ311 (A and B) or AV1451 (C and D), 1 mg/kg injected intravenously 30 min after radiotracer injection. Error bars correspond to standard deviation. Representative transversal images of the baseline experiment with ^{18}F -JNJ311 (B) and ^{18}F -AV1451 (D): averaged image 1-11 min after baseline tracer injection (left) and 90-120 min after tracer injection (right).

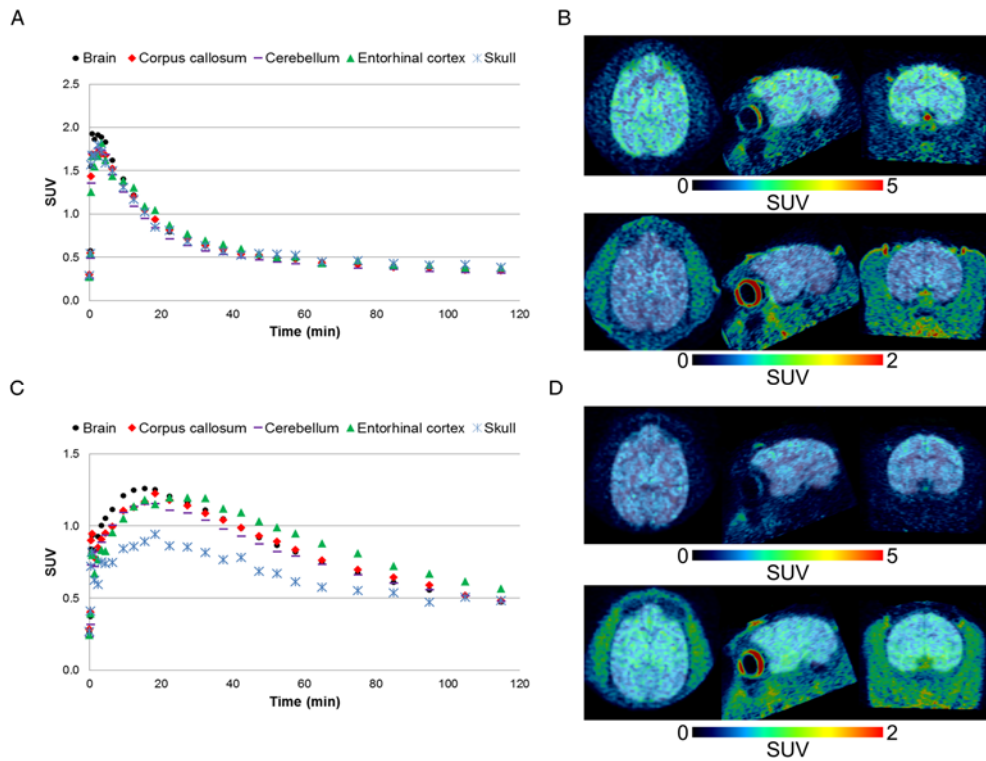


FIGURE 4. μ PET time-activity curves for ^{18}F -JNJ311 (A) and ^{18}F -AV1451 (C) in the whole brain, corpus callosum, cerebellum, entorhinal cortex and skull of a male rhesus monkey. Transversal, sagittal and coronal images of the baseline experiment with ^{18}F -JNJ311 (B) and ^{18}F -AV1451 (D): averaged image 1-10 min after tracer injection (top) and 60-120 min after tracer injection (bottom).

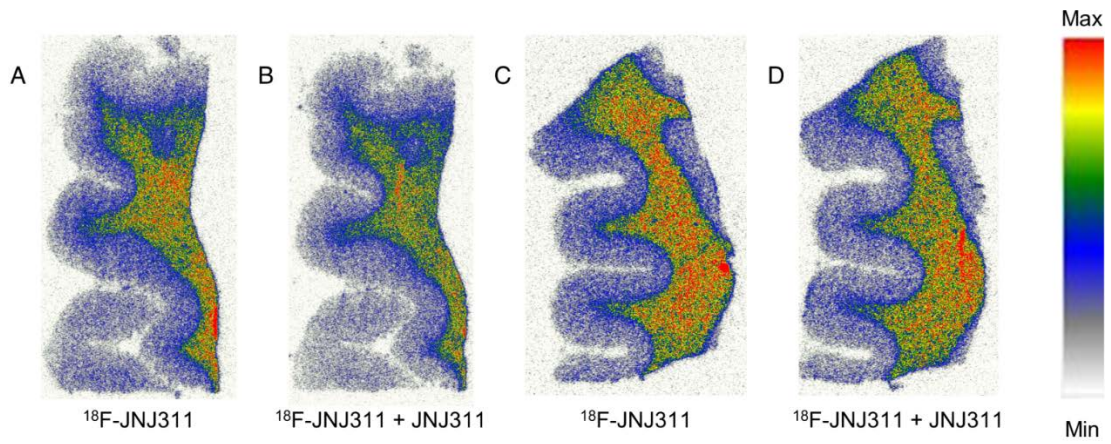
Supplemental Table 1. Human PK predictions for JNJ311.

	Mouse [†]	Rat [†]	Dog [†]	Human
Unbound plasma fraction (%)	36.8	36.9	36.9	37.1
Dose JNJ311 (mg/kg)*	0.25	0.25	0.25	0.25 (pred.)
Plasma clearance (mL/min/kg)	193 ± 63	116 ± 10	77 ± 16	1.05 [‡] , 1.285 [§]
Liver blood flow (%)	> 100	> 100	> 100	-
Volume of distribution at steady state (L/kg)	4.0 ± 0.7	4.5 ± 0.9	4.0 ± 1.0	2.98 [‡] , 3.96 [§]
Elimination half-life (h)	0.3 ± 0.1	0.4 ± 0.1	0.7 ± 0.1	0.7 [‡] , 2.4 [§]
*Formulations with 20% HPβCD aq, [†] values represent mean ± standard deviation from 3 animals, [‡] predicted value using Dedrick approach, [§] predicted value using allometric scaling				

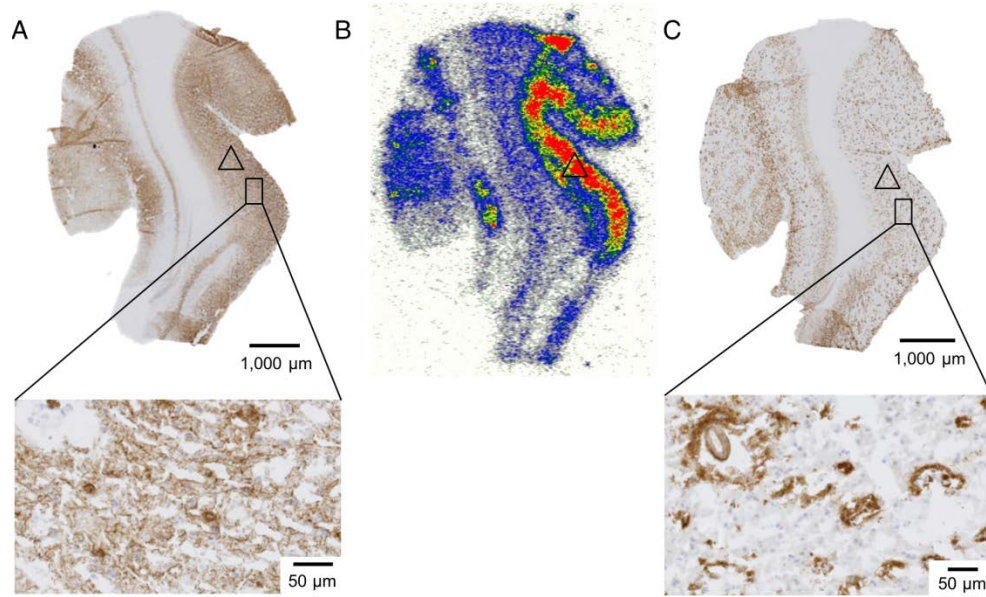
Supplemental Table 2. Biodistribution of ^{18}F -JNJ311 and ^{18}F -AV1451 in NMRI mice at 2, 10, 30 and 60 min p.i.*

Body part	^{18}F -JNJ311				^{18}F -AV1451			
	2 min	10 min	30 min	60 min	2 min	10 min	30 min	60 min
Blood	0.5 ± 0.1	0.3 ± 0.1	0.2 ± 0.0	0.1 ± 0.0	0.4 ± 0.1	0.3 ± 0.0	0.2 ± 0.0	0.2 ± 0.0
Bone	0.5 ± 0.2	0.7 ± 0.1	0.6 ± 0.1	0.5 ± 0.1	0.6 ± 0.4	0.5 ± 0.1	0.7 ± 0.1	0.9 ± 0.2
Brain	1.9 ± 0.1	0.8 ± 0.2	0.3 ± 0.0	0.1 ± 0.0	2.2 ± 0.3	1.0 ± 0.2	0.2 ± 0.1	0.1 ± 0.0
Cerebellum	1.9 ± 0.2	0.7 ± 0.1	0.2 ± 0.1	0.1 ± 0.0	2.4 ± 0.5	0.9 ± 0.2	0.2 ± 0.1	0.1 ± 0.0
Cerebrum	1.9 ± 0.1	0.8 ± 0.1	0.3 ± 0.1	0.1 ± 0.0	2.1 ± 0.3	1.0 ± 0.2	0.3 ± 0.1	0.1 ± 0.0
Heart	2.3 ± 0.8	1.1 ± 0.6	0.4 ± 0.1	0.1 ± 0.1	2.0 ± 0.4	0.8 ± 0.1	0.4 ± 0.1	0.3 ± 0.0
Kidneys	10.6 ± 2.9	8.1 ± 2.5	2.9 ± 0.6	0.9 ± 0.1	10.4 ± 2.4	9.7 ± 1.0	4.9 ± 1.5	3.8 ± 0.7
Liver	2.6 ± 0.6	4.6 ± 0.7	3.4 ± 0.4	1.6 ± 0.3	3.6 ± 0.6	5.6 ± 0.5	6.5 ± 0.6	5.3 ± 0.6
Lungs	8.3 ± 4.6	2.6 ± 1.3	1.0 ± 0.3	0.2 ± 0.1	7.0 ± 2.5	1.6 ± 0.6	1.2 ± 0.3	0.6 ± 0.2
Muscle	1.4 ± 0.1	0.6 ± 0.0	0.2 ± 0.1	0.1 ± 0.0	0.9 ± 0.5	0.5 ± 0.1	0.2 ± 0.0	0.1 ± 0.0
Pancreas	1.4 ± 0.4	1.8 ± 0.4	0.8 ± 0.1	0.2 ± 0.0	1.2 ± 0.6	1.8 ± 0.3	0.7 ± 0.3	0.4 ± 0.1
Spleen	4.9 ± 0.7	2.3 ± 1.0	0.8 ± 0.2	0.2 ± 0.0	4.5 ± 1.6	5.2 ± 4.8	1.2 ± 0.4	0.9 ± 0.4
	2/60 min				2/60 min			
Brain	29.6				18.3			
Blood	7.5				2.4			

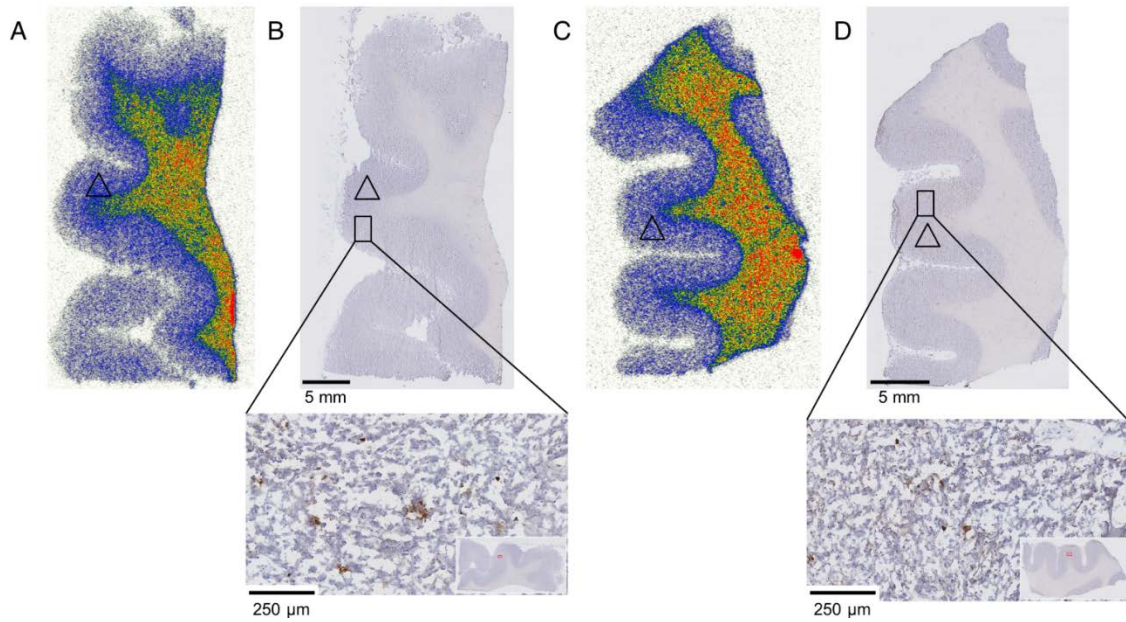
*Data are expressed as SUV mean ± standard deviation; $n = 3$ per time point; ratios were calculated using non rounded values



Supplemental Figure 1. Adjacent, 10- μm -thick, post-mortem human PSP (A and B) and CBD (C and D) brain slices of the frontal cortex of a PSP patient (71-year-old) and CBD patient (74-year-old) incubated with ^{18}F -JNJ311 (740 kBq / 500 μL / slice) (A and C) in the presence of authentic reference compound JNJ311 (B and D) at 1 $\mu\text{mol/L}$.



Supplemental Figure 2. Autoradiographic analysis on 10- μ m-thick slices of the visual cortex of an AD patient (68-year-old with Braak stage VI) with ^{18}F -JNJ311 (B). Adjacent slices were immunostained for tau (A, AT8, 1000- μ m scale bar) and for β -amyloid (C, 4G8, 1000- μ m scale bar). Higher magnification at the bottom identifies tau pathology (50- μ m scale bar) and β -amyloid plaques (50- μ m scale bar). Triangle indicates area of high density of PHF deposits and relatively low density of β -amyloid deposits.



Supplemental Figure 3. Autoradiographic analysis on 10- μ m-thick slices of the frontal cortex of a PSP patient (71-year-old; A and B) and CBD patient (74-year-old; C and D) with ^{18}F -JNJ311 (A and C). Adjacent slices were immunostained for tau (B and D, AT8, 5-mm scale bar). Higher magnification at the bottom identifies tau pathology (250- μ m scale bar). Triangle indicates area of medium density of hyperphosphorylated tau deposits.

Supplemental Table 3. pIC₅₀/K_i (nM) values for purified tau and β-amyloid and molecular features of all compounds.*

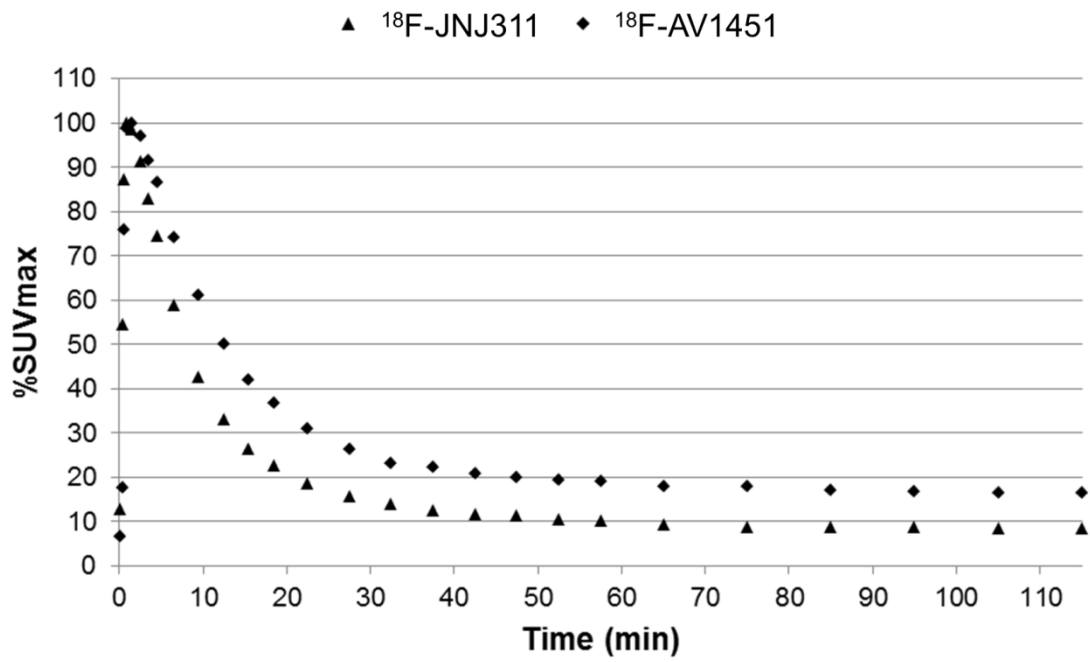
Compound	pIC ₅₀ – tau	K _i – tau	pIC ₅₀ - Aβ	K _i - Aβ	PSA (Å ²) [‡]	LogD _{7.4} [†]
JNJ311	7.7	8	< 5	> 4398	51	2.2
AV1451	8.4	1	6.2	278	42	2.2
AV680	7.7	7	5.0	4934	33	3.0
AV45	5.2	> 2323	7.6	12	53	3.1

*pIC₅₀ values were determined from displacement curves of 2-5 independent experiments, K_i values were calculated from IC₅₀ values using the following equation: $K_i = IC_{50} / (1 + (\text{concentration RL} / K_D \text{ RL}))$, with a K_D for PHF of 6.275 nM for ³H-AV680, a K_D for β-amyloid of 7.85 nM for ³H-AV45, and 10 nM of RL concentration in both assays; [†]LogD_{7.4} value was chromatographically determined for JNJ311, but calculated for the other compounds; [‡]PSA = polar surface area

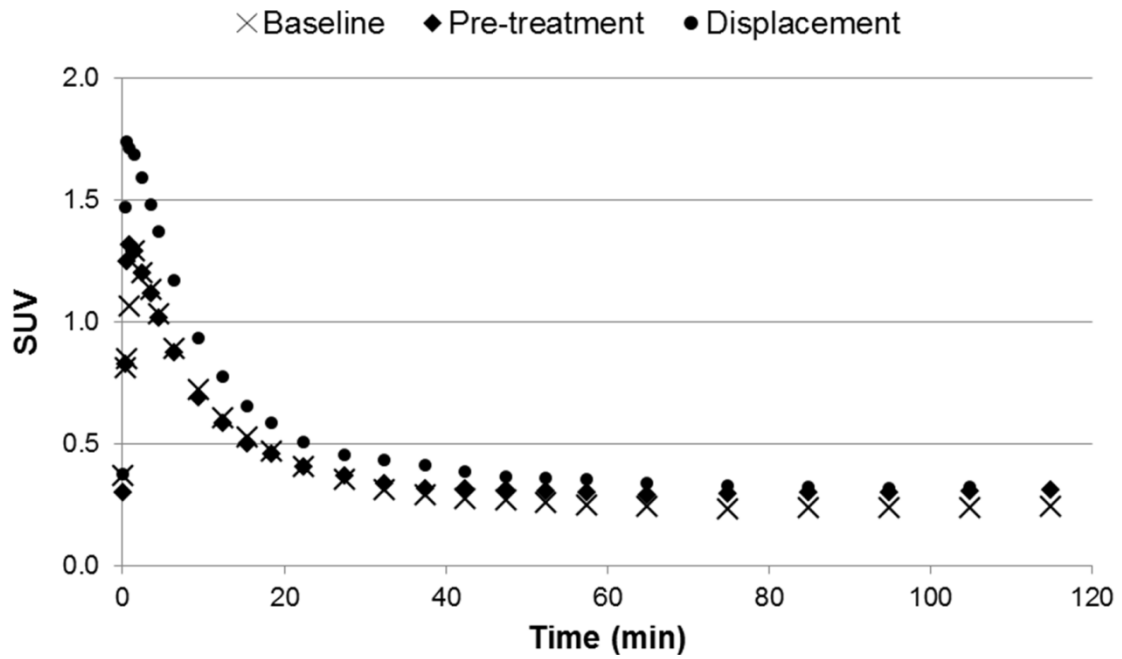
Supplemental Table 4. Relative percentages of intact tracer after i.v. injection of ^{18}F -JNJ311

in plasma of mice and a rhesus monkey and perfused brain of mice.

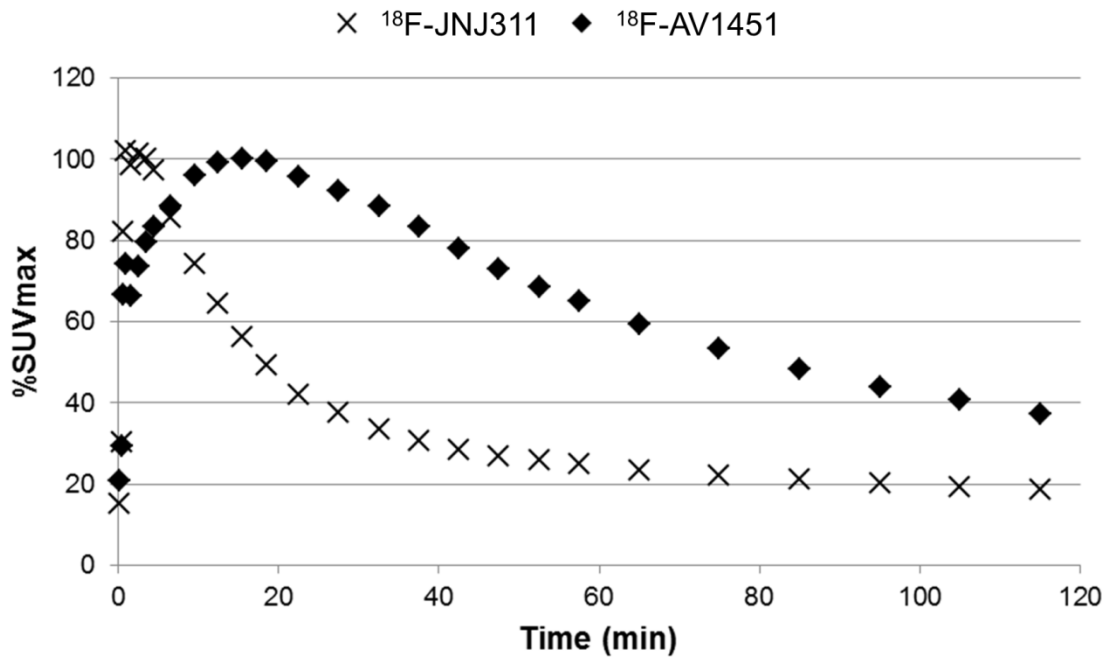
MICE			
Plasma	Mean % \pm standard deviation ($n = 3$) of intact tracer		
<u>2 min</u>	<u>10 min</u>	<u>30 min</u>	<u>60 min</u>
85 \pm 3	33 \pm 6	22 \pm 5	11 \pm 7
Perfused brain	Mean % \pm standard deviation ($n = 3$) of intact tracer		
	<u>10 min</u>		<u>60 min</u>
	98 \pm 0		94 \pm 1
MONKEY			
Plasma	% ($n = 1$) of intact tracer		
	<u>10 min</u>	<u>30 min</u>	<u>60 min</u>
	51	35	28



Supplemental Figure 4. %SUV_{max} curves of small animal μ PET time-activity curves of ¹⁸F-JNJ311 and ¹⁸F-AV1451 in the whole brain of a Wistar rat.



Supplemental Figure 5. Whole brain μ PET time-activity curves for ^{18}F -AV1451 of three female Wistar rats. Baseline scan ($n = 1$); pre-treatment experiment ($n = 1$): pure vehicle, 10 mg/kg injected subcutaneously 60 min prior to radiotracer injection and displacement study ($n = 1$): pure vehicle, 1 mg/kg injected intravenously 30 min after radiotracer injection.



Supplemental Figure 6. Average whole brain %SUV_{max} curves of ¹⁸F-JNJ311 and ¹⁸F-AV1451 in a male rhesus monkey.